

Eleven-orbit inspiral of a mass ratio 4:1 black-hole binary

U. Sperhake^{1,2,3}, B. Brügmann⁴, D. Müller⁴, C. F. Sopuerta¹

¹ Institute of Space Sciences (CSIC-IEEC), Campus UAB, Torre C5 parells, 08193 Bellaterra, SPAIN

² California Institute of Technology, 1200 E California Boulevard, Pasadena, CA 91125, USA

³ Department of Physics and Astronomy, The University of Mississippi, University, MS 38677-1848, USA

⁴ Theoretisch Physikalisches Institut, Friedrich Schiller Universität, Max-Wien Platz 1, 07743 Jena, Germany

E-mail: sperhake@ieec.uab.es

Abstract. We analyse an eleven-orbit inspiral of a non-spinning black-hole binary with mass ratio $q \equiv M_1/M_2 = 4$. The numerically obtained gravitational waveforms are compared with post-Newtonian (PN) predictions including several sub-dominant multipoles up to multipolar indices ($l = 5, m = 5$). We find that (i) numerical and post-Newtonian predictions of the phase of the (2,2) mode accumulate a phase difference of about 0.35 rad at the PN cut off frequency $M\omega = 0.1$ for the Taylor T1 approximant when numerical and PN waveforms are matched over a window in the early inspiral phase; (ii) in contrast to previous studies of equal-mass and specific spinning binaries, we find the Taylor T4 approximant to agree less well with numerical results, *provided* the latter are extrapolated to infinite extraction radius; (iii) extrapolation of gravitational waveforms to infinite extraction radius is particularly important for subdominant multipoles with $l \neq m$; (iv) 3PN terms in post-Newtonian multipole expansions significantly improve the agreement with numerical predictions for sub-dominant multipoles.

The research area of Gravitational Wave (GW) Physics has acquired enormous momentum in the course of the last decade. The ground-based detectors LIGO, VIRGO and GEO600 have operated at design sensitivity and the former two are currently being upgraded to advanced status [1, 2]. Simultaneously, the planned ESA/NASA space mission LISA will soon enter a crucial stage with the launch of the precursor mission LISA Pathfinder [3]. Progress in theoretical GW source modelling has mirrored that on the experimental side. Most importantly, the general relativistic two-body problem for comparable-mass systems has been solved using numerical relativity (NR) techniques [4, 5, 6], leading to a wealth of insight into the dynamics of black-hole binaries [7, 8].

In order to maximise the scientific output of the expected gravitational wave observations, it is crucial to have available catalogues of highly accurate gravitational waveform templates which are then used via the *matched filtering* technique [9] to dig out physical signals from the observed data stream. The construction of such waveform templates currently follows either of the two following strategies. *Phenomenological template banks* are based on *hybrid waveforms* combining post-Newtonian predictions

for most of the inspiral with numerical relativity results for late inspiral, merger and ringdown. Phase and amplitude are then assumed to be well-approximated by relatively simple functions of the binary parameters and the GW frequency ω . Free parameters in these functions are determined by comparison with a finite number of hybrid waveforms. This approach, initially presented in [10, 11, 12] has been applied to a subset of spinning configurations in [13, 14, 15, 16]. The second approach, the *effective-one-body method* (EOB) [17], targets at semi-analytic predictions for the entire waveform via matching post-Newtonian results to an effective-one-body metric and thus models the binary through merger and ring-down. Again, free parameters in the matching are determined by comparison with a finite set of numerical relativity simulations. Applications of the EOB method can be found, for example, in [18, 19, 20, 21, 22] for non-spinning and in [23] for non-precessing spinning binaries.

Clearly, both approaches are heavily dependent on high-precision numerical relativity results. Length requirements for the numerical simulations in the context of gravitational wave detection have been studied for non-spinning binaries and special spin configurations in [24] and are in the range of about ten orbits. A recent study on accuracy requirements for detection efficiency and parameter estimation by MacDonald *et al.* [25] employs criteria developed in [26, 22] and reports a larger number of about 30 orbits required for hybridisation with current post-Newtonian waveforms; for more details see these articles and references therein. Finally, we note that numerical relativity waveforms are directly used in GW data analysis inside the *Ninja* project [27, 28].

Purpose of our paper is to study in detail the accuracy of an eleven-orbit inspiral of a non-spinning black-hole binary with mass ratio $q = 4$ obtained with the LEAN code [29]. While higher-order multipoles have been investigated in the context of the EOB model [30, 31] and PN-NR comparisons in [32, 33, 34, 35], we are not aware of their inclusion in the construction of phenomenological models of hybrid PN-NR waveforms. In this work, we will compare our numerical results for the quadrupole as well as several subdominant modes with the Taylor T1 and T4 approximants and different PN multipolar expansions.

We start this paper with a brief summary of the numerical framework in Sec. 1. The simulations and the numerical error analysis is presented in Sec. 2. In Sec. 3 we discuss the different post-Newtonian approximants used in this work and the method to construct hybrid waveforms. These are analysed in Sec. 4 and we conclude in Sec. 5.

1. Computational framework

The initial data for our black-hole binary configurations are constructed according to the puncture method [36]. Specifically, we use the analytic Bowen-York extrinsic curvature [37] with linear momentum \mathbf{P} and solve the Hamiltonian constraint for the conformal factor using the spectral solver of Ansorg *et al.* [38]. In order to reduce the eccentricity of the binary system, we determine the non-vanishing radial component P_{rad} of the initial momentum via the iterative procedure described in Ref. [39].

The initial parameters thus obtained are given in units of the total black-hole mass $M = M_1 + M_2$ in Table 1. The bare mass parameters have been chosen such that the irreducible masses as calculated with Thornburg's AHFINDERDIRECT [40, 41] correspond exactly to a binary with mass ratio $q = 4$. For completeness we also give the final spin of the merged hole and the recoil velocity. The latter is in excellent agreement with the prediction $v_{\text{kick}} = 156.9$ km/s by [42], confirming that the early

Table 1. Initial bare mass parameters m_1 , m_2 , location x_1 , x_2 and tangential and radial linear momentum of black holes 1 and 2 of the binary. v_{kick} and j_{fin} are the kick velocity and spin of the post-merger hole.

m_1/M	m_2/M	x_1/M	x_2/M	P_{tan}/M	P_{rad}/M	v_{kick}	j_{fin}
0.7923	0.1913	2.1865	-8.746	± 0.05805	$\mp 3.894 \times 10^{-4}$	156.6 km/s	0.473

inspiral does not significantly contribute to the recoil; cf. the discussion in Sec. III C of [43].

These initial data are evolved in time with the so-called *moving puncture* framework [5, 6] using the LEAN code [29] with upgrades to sixth-order spatial discretization as summarised in Sec. III of Ref. [44]. The LEAN code is based on the CACTUS computational toolkit [45] and employs mesh refinement provided by CARPET [46, 47]. The exact implementation of the Baumgarte-Shapiro-Shibata-Nakamura (BSSN) [48, 49] formulation of the Einstein equations is given by Eqs. (A1), (A4), (A6-A8) of [29]. We further impose a *floor* value $\chi_{\text{floor}} = 10^{-4}$ on the conformal factor; cf. [5]. The gauge variables are initialised as vanishing shift $\beta^i = 0$ and a precollapsed lapse $\alpha = \sqrt{\chi}$, where $\chi = (\det \gamma_{ij})^{-1/3}$ and γ_{ij} is the three metric. Lapse and shift are evolved according to Eqs. (17) and (26) of Ref. [50] with a damping parameter $\eta = 1.75/M$.

The computational domain consists of a set of five nested boxes centred on the coordinate origin and five additional refinement levels with two components each, centred on the black holes. In terms of the notation in Sec. II E of [29], the exact grid setup is given in units of M by

$$\{(307.2, 153.6, 102.4, 32, 16) \times (3.2, 1.6, 0.8, 0.4, 0.2), h_i\}$$

with resolutions $h_0 = M/160$, $h_1 = M/180$, $h_2 = M/200$, $h_3 = M/220$ and $h_4 = M/240$ for studying the convergence properties. The lowest resolution simulation using h_0 becomes unstable due to a gauge instability at the outermost refinement boundary at about $t = 1700 M$; see [51, 52, 53, 54] for more in-depth discussion and cures of this instability. While we do not use this simulation directly for comparison with post-Newtonian predictions, it extends sufficiently far into the inspiral to provide consistency checks of our convergence results.

Gravitational waves are extracted in the form of the Newman-Penrose scalar Ψ_4 at radii $r_{\text{ex}} = 64 M, 72 M, 80 M, 88 M, 96 M, 104 M$ and $112 M$ using the method described in Appendix C in [29]. The resulting Ψ_4 is decomposed into multipoles ψ_{lm} by projection onto spherical harmonics of spin-weight -2 according to Eq. (2.1) of Ref. [33]; see also [55] for sign conventions.

Our analysis of the gravitational waves will use the gravitational wave strain h which is related to the Newman-Penrose scalar by

$$\Psi_4 = \ddot{h}_+ - i\ddot{h}_\times. \quad (1)$$

The multipoles H_{lm} of the strain are related to those of Ψ_4 by Eq. (II.5) of Brown *et al.* [56], that is, two integrations in time of ψ_{lm} . These integrations in time represent a non-trivial operation and often result in low frequency drifts [33, 57]. In order to circumvent these problems, we use a modified version of the integration in Fourier space as originally introduced in Ref. [58], see also [35]: the Fourier transform $\tilde{H}_{lm}(\omega)$ is divided by $-\omega^2$, but set to zero inside a specified window. Our modification consists

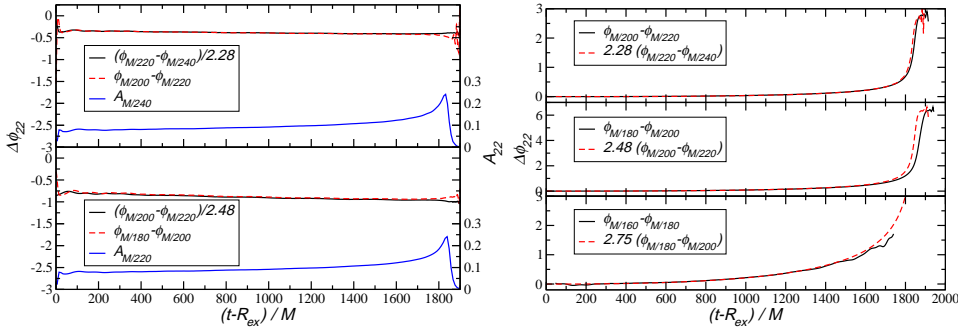


Figure 1. Convergence of the phase ϕ_{22} for resolutions h_1 , h_2 , h_3 and h_4 and aligning the waveforms at the maximum of the (2, 2) mode (left panel) and for resolutions h_0 , h_1 , h_2 , h_3 and h_4 and aligning the waveforms at the start of the numerical simulation (right panel). The scaling factors correspond to eighth-order convergence. The lower solid curve in the left panel represents the amplitude A_{22} and serves as orientation.

in smoothing the filter function from Heaviside shape to

$$g(x) = \begin{cases} 0 & x < 0 \\ \frac{1}{\mathcal{N}} \int x^4 (1-x)^4 dx & 0 < x < 1 \\ 1 & x > 1 \end{cases} \quad (2)$$

where $x = (\omega - \omega_0)/\Delta\omega$ and \mathcal{N} is a normalisation constant. For the present study, we empirically find $M\omega_0 = 0.001$ and $M\Delta\omega = 0.001$ to provide satisfactory results.

2. Numerical results

Before analysing the physical properties of the binary evolution, we estimate the uncertainties due to discretization and wave extraction at finite radii. The convergence of the phase ϕ obtained from the $l = 2$, $m = 2$ multipole is shown in Fig. 1 for all resolutions h_i , $i = 0, \dots, 4$. For the results in the left panel, we have aligned the waveforms in time at $t_{A_{22}}$, the time of the peak of the amplitude of the (2,2) multipole. Those displayed in the right panel are obtained for aligning the waveforms at t_0 , the start of the simulation[‡]. The results are consistent with eighth-order convergence for all resolutions employed. Similarly, we observe eighth-order convergence for the amplitude. Bearing in mind that most of the discretization in our code is sixth-order, it appears that the leading-order discretization errors are subdominant. Whether this occurs due to systematic cancellation is hard to identify because of the enormous complexity of the Einstein equations. In order to test whether the observed convergence is coincidental or systematic, we have performed the larger set of runs employing five different resolutions and using different choices of aligning the waveforms in time. The observation of the same clean convergence order for all cases demonstrates the robustness of our observations. For the determination of uncertainties due to discretization, however, we will calculate Richardson extrapolated results using a more conservative sixth-order extrapolation.

The deviations of phase and amplitude obtained at finite resolutions from the Richardson extrapolated values are shown in Fig. 2 for both types of alignment of the

[‡] The lowest resolution simulation has only been used in the latter case because it does not extend to the maximum of the amplitude of the (2,2) mode.

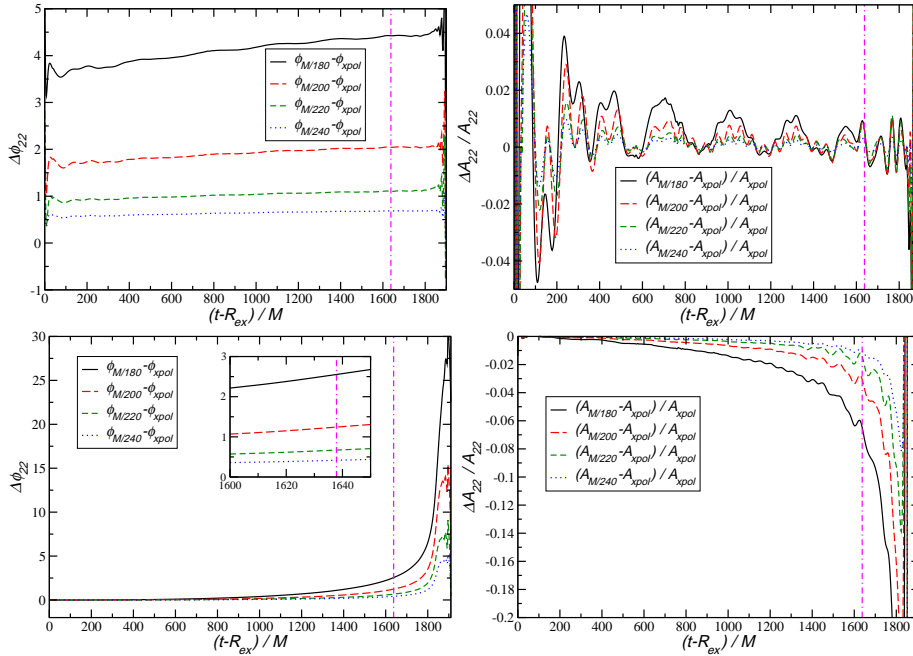


Figure 2. Deviation of the phase ϕ (left) and relative deviation of the amplitude (right panel) obtained for finite resolution from the Richardson extrapolated values and for aligning the waveforms at $t_{A_{22}}$, the maximum of the amplitude of the (2,2) multipole (upper panels) and at the start of the simulation t_0 (lower panels). The vertical lines mark the time t_w where the frequency of the (2,2) multipole reaches $M\omega_{22} = 0.1$.

waveforms, at $t_{A_{22}}$ (upper panels) and at t_0 (lower panels). For the former alignment, the figure implies a phase error of $\Delta\phi \lesssim 0.6$ rad for the high-resolution simulation. We note, however, that the phase difference between the high resolution and the extrapolated result is nearly constant until the late ringdown stage. Because a constant phase offset does not enter the comparison with PN results, the relevant phase error for this purpose is given by the variation of the difference over the simulation which is significantly smaller, about $\Delta\phi \approx 0.11$ rad. The relative amplitude error shown in Fig. 2 is less than 1 % and, as we shall see below, dominated by the uncertainty arising from the use of finite extraction radii.

In case of aligning the waveforms at t_0 , Fig. 2 implies an accumulated phase error of about 0.4 rad for the phase of the high resolution run at t_w defined as the time when the frequency of the multipole reaches $M\omega_{22} = 0.1$, the endpoint of the post-Newtonian integration in Sec. 3 (vertical lines in the figure). The amplitude error has grown to 2 % at the same time. We note here that alignment of the gravitational waves at $t_{A_{22}}$ results in smaller uncertainty estimates. For the analysis of Sec. 4, however, estimates obtained for both type of alignments are adequate. In that analysis we will exclusively use the high-resolution data set.

In order to estimate the error due to finite extraction radius, we assume a polynomial dependence of the phase error on $1/R_{\text{ex}}$ [59]. While the linear term is expected to dominate the error, in practise the quadratic term may also be significant

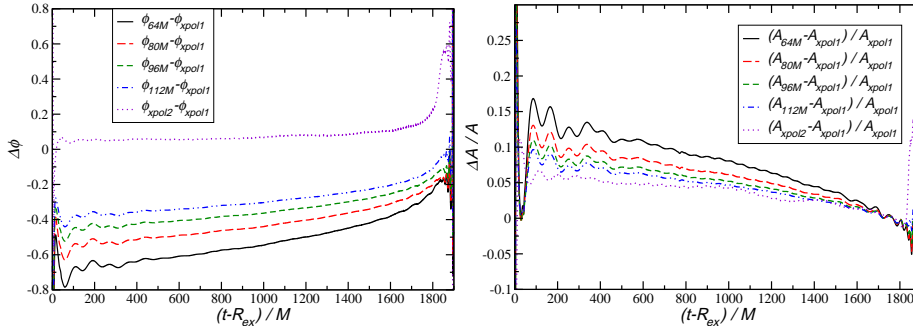


Figure 3. Deviation of the phase ϕ (left) and relative deviation of the amplitude (right panel) obtained at finite extraction radius from the values extrapolated according to Eq. (3).

[60]. We therefore fit the numerical data assuming either of

$$f(r) = f_0 + \frac{f_1}{r}, \quad (3)$$

$$f(r) = f_0 + \frac{f_1}{r} + \frac{f_2}{r^2}, \quad (4)$$

and denote the extrapolated results thus obtained “xpol1” and “xpol2”, respectively. Eventually, we use the extrapolated result “xpol1” in the analysis below and estimate the error by its deviation from the “xpol2” result. These deviations are shown for phase and amplitude and a subset of all extraction radii in Fig. 3. From the figure we infer a relative error of 5 % or less for the amplitude while the phase error is ≤ 0.2 rad up to merger and increases to about 0.5 rad in the late ringdown stage.

The phase uncertainties of higher order multipoles behave similarly to those of the quadrupole, but we find the overall errors to scale approximately with the multipole index m . The amplitude errors of subdominant modes are significantly larger, however, due to the lower signal combined with numerical noise. Extrapolation of the amplitude to infinite extraction radius amplifies the numerical noise and we therefore present higher order multipoles using extrapolated phase, but amplitude from the largest extraction radius instead. The numerical uncertainties of these amplitudes are about 12 % for the (3, 3) mode, 20 % for the (4, 4) and (5, 5) mode and 25 % for the (3, 2) and (4, 3) mode. While these errors are too large for a high precision study, they will allow us to calibrate the significance of 3PN order terms in the post-Newtonian multipole expansion in Sec. 4.

The errors stated so far are internal checks of accuracy. For the purpose of an external verification of our results, we compare the amplitude and phase of the $l = 2$, $m = 2$ mode to results obtained with the independent BAM code [61, 55]. In order to avoid additional uncertainties arising from the integration of the Newman-Penrose scalar Ψ_4 to strain h , here we compare the modes of Ψ_4 which we directly obtain from the numerical simulations in both codes. The BAM simulations also use lower resolutions (hence the larger uncertainties) and different extraction radii. We therefore present this comparison using results extrapolated both in resolution, assuming second order convergence for the BAM runs, and extraction radius, using Eqs. (3), (4).

The uncertainties of the BAM simulation are studied in detail in [62] and are

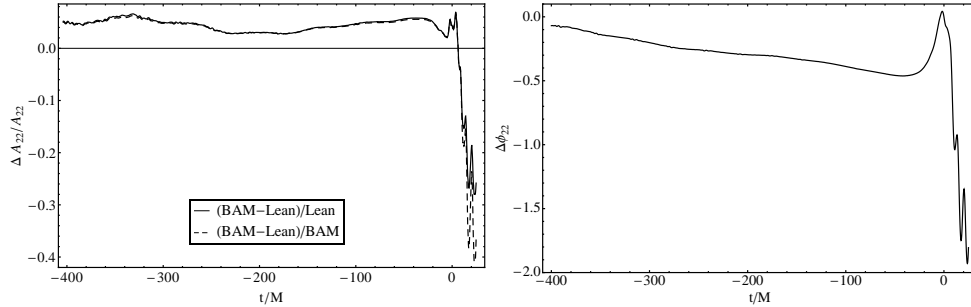


Figure 4. Relative amplitude differences (left panel) and phase differences (right panel) of the $l = 2$, $m = 2$ modes of Ψ_4 between the extrapolated (in resolution and extraction radius) results from the BAM and the LEAN codes. Results from both codes are aligned at the time of peak amplitude $t_{A_{22}}$. We note that the relatively large percentage discrepancy between the results of the two codes at late times is a consequence of the very low amplitude of the wave signal in the late ringdown.

summarised as follows. The accumulated phase error for the $N = 96$ high resolution run at t_ω as obtained from Richardson extrapolation and for aligning the waveforms at t_0 is 0.46 rad and the error due to the use of finite extraction radius at $R_{\text{ex}} = 90 M$ is 0.15 rad. The corresponding uncertainty in the amplitude is about 10 % for both, discretization and finite extraction radius during the inspiral and merger.

Relative deviations between the amplitudes and phase differences obtained from the two codes are shown in Fig. 4. Note that the waveforms have been aligned at $t_{A_{22}}$ defined as $t \equiv 0$ on the horizontal axes of this figure. This alignment becomes necessary because of the different initial separations (and, hence, duration) of the simulations, $D = 10 M$ for BAM and $D = 11 M$ for LEAN. Phase and amplitude differences shown in the figure are well within the uncertainty estimates of the two simulations.

Finally, we evaluate the residual eccentricity of the binary simulated with LEAN as a function of time according to [63]

$$e_\phi(t) = \frac{\phi_{\text{NR}}(t) - \phi_{\text{fit}}(t)}{4}, \quad (5)$$

where ϕ_{NR} is the phase of the numerical $(2, 2)$ mode and ϕ_{fit} a seventh order polynomial fit of this phase over a time window $t - R_{\text{ex}} = 250 \dots 1600 M$. We thus obtain an oscillatory pattern of $e_\phi(t)$ with an amplitude gradually decreasing from 0.005 early on towards 0.002 one to two orbits before merger.

3. Post-Newtonian approximants and hybrid waveforms

Post-Newtonian waveforms are calculated using the so-called *Taylor T1* and *Taylor T4* approximants; cf. [59] for a summary including further approximants. Frequency and phase are obtained from the system of ordinary differential equations

$$\frac{dx}{dt} = -\frac{\mathcal{L}}{dE/dx}, \quad (6)$$

$$\frac{d\Phi}{dt} = \frac{1}{M} x^{3/2}. \quad (7)$$

Here x is related to the orbital frequency via $x \equiv (M\Omega)^{2/3}$, Φ is the orbital phase, and the gravitational wave flux \mathcal{L} and the orbital energy E are given by Eqs. (231) and (203), respectively, of Blanchet's review [64]. The difference between the Taylor T1 and Taylor T4 approximant is the treatment of the right hand side of Eq. (6). The former calculates the quotient $\mathcal{L}/(dE/dx)$ numerically from the PN truncated individual expressions for numerator and denominator while the T4 approximant expands the quotient in a series in x and truncates this series at the appropriate PN order, 3.5 in our case. The two approximants thus differ only at higher PN order, but previous studies have found the Taylor T4 approximant to produce particularly good agreement with numerical results [59, 62].

In either case, we obtain the rescaled frequency x and the orbital phase Φ from integration of Eqs. (6) and (7). The gravitational wave multipoles are given in terms of these quantities by Kidder's Eqs. (79)-(116) in [65] (to 3PN order for (2, 2) and (4, 4) and 2.5PN order otherwise) or Eq. (9.4) of the more recent study by Blanchet *et al.* [66] (to 3PN order). Unless specified otherwise, results displayed use the latter 3PN terms.

In order to construct a hybrid waveform, we need to determine the integration constants Φ_0 and t_0 of the system (6), (7). In practise, this is achieved by maximising the overlap between the real part of the post-Newtonian multipole $H_{22,\text{PN}}$ and its numerical counterpart $H_{22,\text{NR}}$ over a matching window $t_1 \leq t - R_{\text{ex}} \leq t_2 M$. In this context, the overlap of two functions f and g is defined as

$$\xi \equiv \frac{\langle f, g \rangle}{\sqrt{\langle f, f \rangle \langle g, g \rangle}}, \quad (8)$$

$$\langle f, g \rangle \equiv \int_{t_1}^{t_2} f(t) g(t) dt. \quad (9)$$

The maximisation is achieved using the downhill simplex method of Nelder & Mead [67, 68]. Finally, we combine the PN and numerical waveform into a hybrid according to

$$H_{lm} = (1 - w)\alpha H_{lm,\text{PN}} + w H_{lm,\text{NR}}, \quad (10)$$

where the weighting function $w = 1$ for $t < t_1$, $w = 0$ for $t > t_2$ and for values $t_1 < t < t_2$ a smooth transition is given by

$$w = 630 \left(\frac{1}{9} z^9 - \frac{1}{2} z^8 + \frac{6}{7} z^7 - \frac{2}{3} z^6 + \frac{1}{5} z^5 \right), \quad (11)$$

$$z \equiv \frac{t - t_1}{t_2 - t_1}. \quad (12)$$

The additional factor α has been introduced to compensate for differences in the amplitude between the post-Newtonian and numerical results. For each multipole it is chosen such that the average PN wave amplitude inside the interval $[t_1, t_2]$ matches the NR result.

In order to test the robustness of our results versus the details of the matching procedure, we perform an alternative matching by equating phase and time at a fiducial point in time chosen to be t_w where the gravitational wave frequency of the (2,2) mode takes the value $M\omega_{22} = 0.1$.

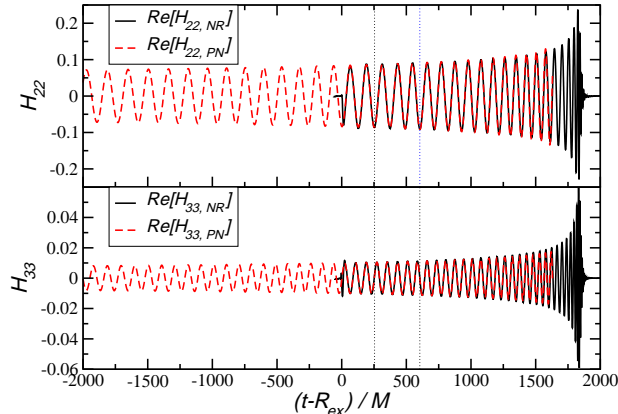


Figure 5. Real part of the $l = 2$, $m = 2$ and the $l = 3$, $m = 3$ gravitational wave modes. The Taylor T1 PN waveforms (dashed) are matched to the numerical results in the window $250 M \leq t - R_{\text{ex}} \leq 600 M$ indicated by vertical dotted lines.

4. Analysis

The results of the matching procedure using a window $t_1 = 250 M$, $t_2 = 600 M$ are illustrated for the Taylor T1 approximant in Fig. 5, which shows the real part of the $(2, 2)$ and the $(3, 3)$ modes. The matching window is indicated by the vertical dotted lines. The corresponding figure for Taylor T4 would look nearly identical.

In order to quantitatively analyse the agreement between the PN and NR results, we display in Fig. 6 the phase differences for various multipoles obtained by using the Taylor T1 (left panels) and T4 (right panels) approximants and numerical results extracted at $R_{\text{ex}} = 64 M$ and $96 M$ as well as extrapolated to infinite extraction radius. For orientation we plot near the bottom of each panel the gravitational wave frequency $M\omega_{22}$ of the $l = 2$, $m = 2$ mode (dash-dash-dotted curve). All curves end at $M\omega_{22} = 0.1$ which is the maximum frequency chosen for the PN integration.

We begin our discussion with the dominant quadrupole mode $l = 2$, $m = 2$. In all cases, the phase agreement between PN and NR results is better than $\Delta\phi = 0.1$ rad inside the matching window, but gradually increases as the inspiral proceeds until the accumulated phase discrepancy reaches values between 0.25 rad and 0.75 rad. At both finite extraction radii the agreement grows to larger values for the Taylor T1 expansion than the T4 approximant. The behaviour of the $(3, 3)$, $(4, 4)$ and $(5, 5)$ modes is similar, although with larger phase discrepancy approximately proportional to the multipole index m . This is not too surprising bearing in mind that the phase grows faster for higher-order modes with the same proportionality.

Those subdominant multipoles with $l \neq m$, however, exhibit a drastically different behaviour when extracted at finite radius. For both, the $(3, 2)$ and the $(4, 3)$ mode the numerical phase differs significantly from the PN predictions throughout the entire simulation. We note, in this context, that the orbital phase in the PN expressions is fixed exclusively using information from the $(2, 2)$ mode. Furthermore, inspection of the post-Newtonian multipoles in Refs. [65] and [66] reveals that the $(2, 2)$ and the $(3, 2)$ GW multipoles are almost in phase[§]. Indeed, this is also the case for the

[§] The minor dephasing due to the complex PN amplitudes of the $(2, 2)$ and $(3, 2)$ modes is negligible

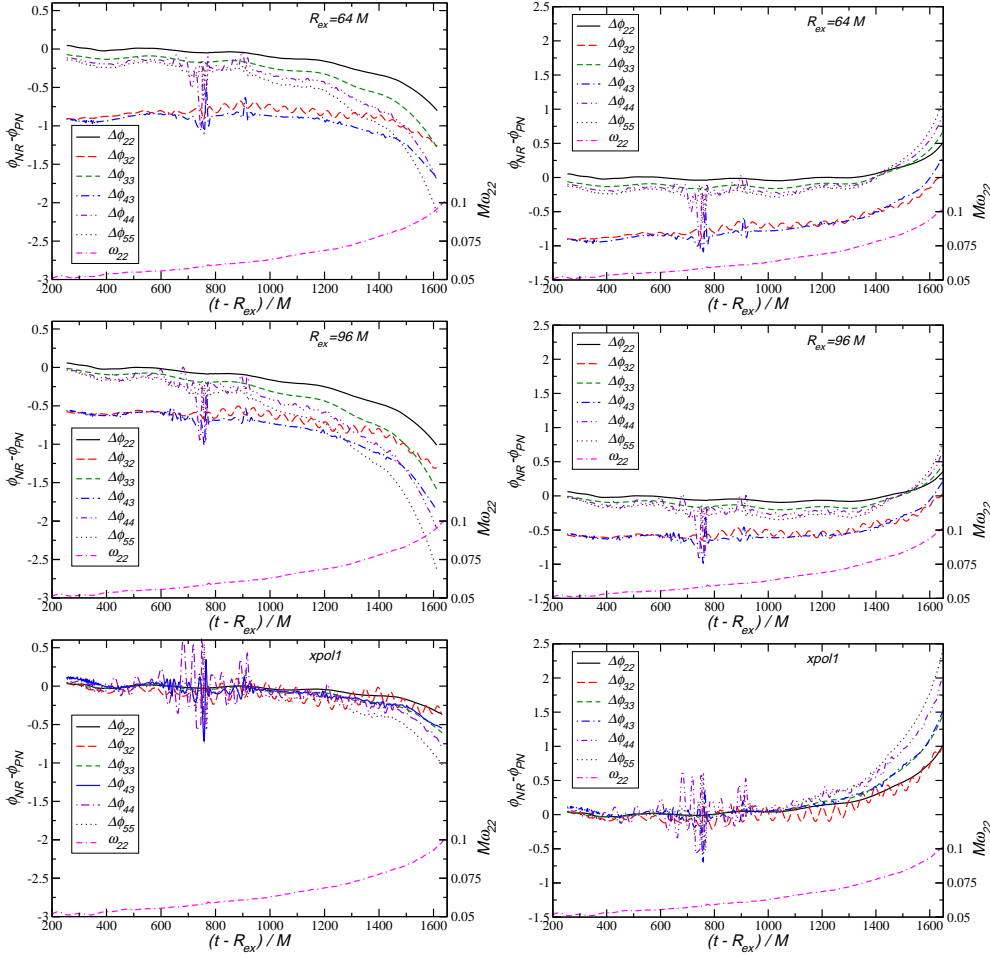


Figure 6. Phase difference between the PN and NR results obtained by using a matching window with $t_1 = 250 M$ and $t_2 = 600 M$ and numerical results at (from top to bottom) $R_{\text{ex}} = 64 M$, $96 M$ and extrapolated to infinity. Results in the left column are obtained for the Taylor T1 expansion, those on the right for Taylor T4. The dash-dash-dotted curve near the bottom of each panel gives the GW frequency of the (2, 2) mode for reference.

numerical modes *provided* we extrapolate to infinite extraction radius, as becomes apparent in the bottom panels where the large phase error of the (3, 2) and (4, 3) modes disappear. We also illustrate this feature in Fig. 7 where we plot the real part of the numerical (2, 2), (3, 2) and (4, 2) modes^{||}. The figure demonstrates that (i) the dephasing is largest for the (4, 2) mode, (ii) the dephasing decreases at larger extraction radius and (iii) the dephasing virtually disappears if we extrapolate to infinite extraction radius. We make exactly the same observations for the (4, 3) and the (3, 3) multipoles; see the short-dashed and dash-dotted curves in Fig. 6. Our findings

in this context.

^{||} The low amplitude of the (4, 2) combined with numerical noise prevent us from performing accurate extrapolation to infinite extraction radius which is also the reason it is not included in the remainder

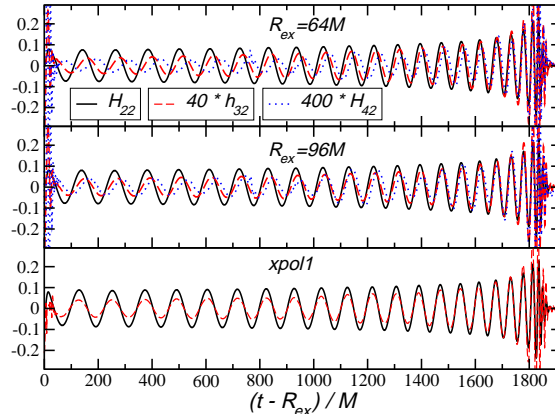


Figure 7. The (2,2) (solid), (3,2) (dashed) and (4,2) (dotted) multipole extracted at $R_{\text{ex}} = 64 M$ and $96 M$ (upper panels) and the former two extrapolated to infinite extraction radius (bottom panel).

demonstrate the importance of having available either reliable wave extraction tools at future null infinity [69, 70, 71] or accurate extrapolations from results at finite radii [72].

A further interesting feature of the extrapolated modes is the significant improvement of the phase agreement between NR and the Taylor T1 approximant; for $R_{\text{ex}} \rightarrow \infty$, Taylor T1 provides better agreement than T4. We thus cannot confirm for our unequal-mass binary the exceptional behaviour of the T4 approximant reported for the equal-mass case by [59] and a $q = 4$ unequal-mass binary in Fig. 8 of Ref. [62]. We note, however, that this does not constitute an incompatibility of our results with those of Ref. [62], because the latter are based on waveforms at finite extraction radius $90 M$, where we also obtain better agreement of numerical results with T4.

We next perform the following tests in order to investigate the robustness of our observations at infinite extraction radius. (i) Motivated by the observation of noise in the numerical phase due to spurious initial radiation in the earlier part of their waveform in Ref. [21], cf. their Fig. 17¶, we choose a later matching window $t_1 = 900 M$, $t_2 = 1250 M$. (ii) Instead of using a window, we match phase and time at the fiducial point in time t_ω where $M\omega_{22} = 0.1$ as done for example in Ref. [62]. (iii) We apply the matching procedure with $t_1 = 250 M$, $t_2 = 600 M$ to the BAM waveform. The results are shown, from top to bottom, in Fig. 8. As expected, different alignment procedures produce different functions of time for the phase differences. But for all cases, we observe better agreement of the numerical simulations with the Taylor T1 prediction as compared with Taylor T4. This is also the case for the BAM simulation which is furthermore consistent within the respective uncertainties with that obtained with the LEAN code. We conclude that the exceptional agreement of Taylor T4 observed for some specific black-hole configurations is most likely explained by a coincidental cancellation of higher-order post-Newtonian corrections which does not hold for general systems.

of this study.

¶ We note that Boyle *et al.* use different initial data and that the amplitude of the noise is at least one order of magnitude below the effects investigated in our work, compatible with the absence of such noise in the (2,2) mode on the scale of our Fig. 6.

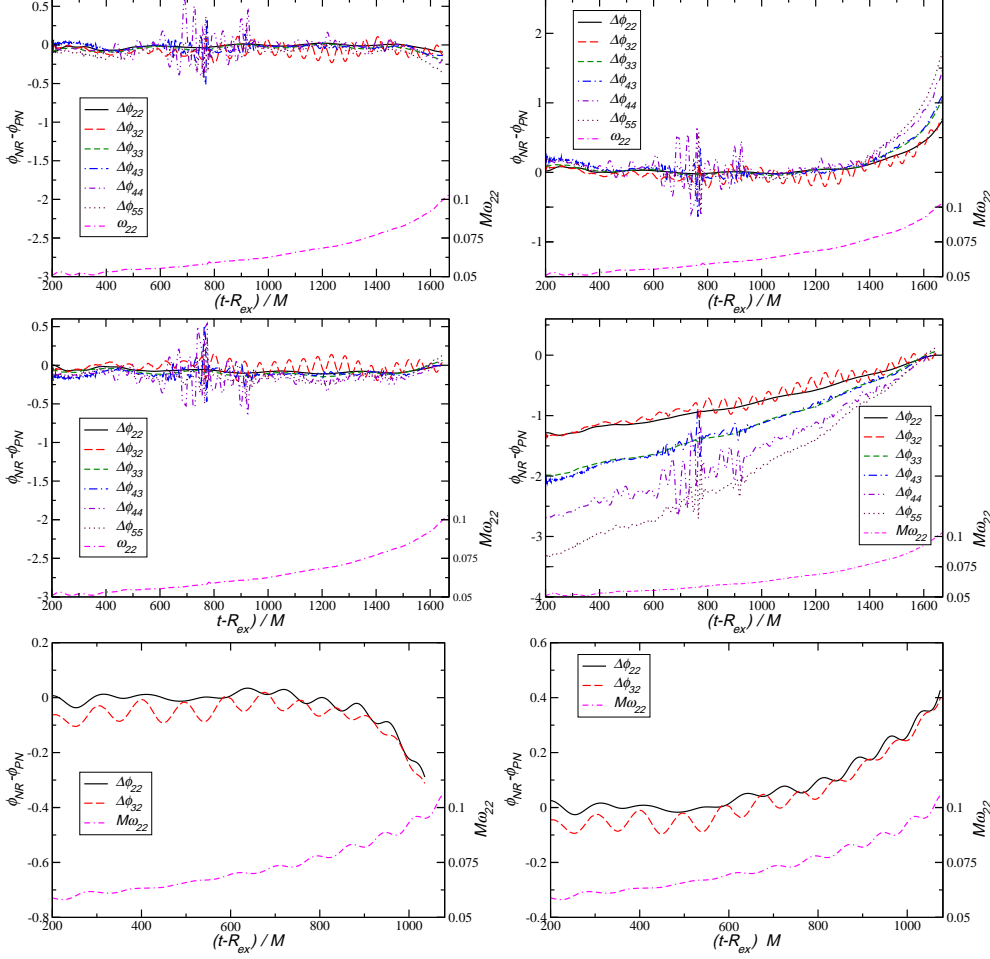


Figure 8. Phase difference between the PN and NR results obtained by using numerical results extrapolated to infinity and employing a later matching window $t_1 = 900 M$, $t_2 = 1250 M$ (upper panels), matching phase and time at a fiducial point in time where $M\omega_{22} = 0.1$ (centre panels) and using a matching window $t_1 = 250 M$, $t_2 = 600 M$ for $(2,2)$ and $(3,2)$ multipoles of the BAM simulation (bottom panels). Results in the left column are obtained for the Taylor T1 expansion, those on the right for Taylor T4. The dash-dash-dotted curve near the bottom of each panel gives the GW frequency of the $(2,2)$ mode for reference.

Finally, we consider differences in the amplitude predictions of post-Newtonian and numerical relativity results. The PN expressions for the gravitational wave multipoles in Refs. [65] and [66] differ in the inclusion of higher order terms in several subdominant modes in the latter work. In order to assess the significance of these higher-order terms, we have performed the matching of numerical to PN waveforms as described in Sec. 3 with $t_1 = 250 M$ and $t_2 = 600 M$ using either set of multipole expressions. As mentioned above, the matching process involves a rescaling of the PN waveforms to compensate for amplitude differences in the matching window, the factor α in Eq. (10). For all subdominant multipoles which have been extended to 3PN order in [66], we observe in Table 2 an improvement in the agreement between NR and PN

Table 2. Deviations of the rescaling factor α introduced in Eq. (10) from unity for several multipoles and using the multipole expressions of Ref. [65] or Ref. [66] which includes higher-order PN terms for subdominant modes.

(l, m)	(2, 2)	(3, 3)	(3, 2)	(4, 4)	(4, 3)	(5, 5)
$\alpha - 1$ (T1, [65])	0.047	-0.071	-0.065	-0.108	0.251	0.712
$\alpha - 1$ (T1, [66])	0.047	0.023	-0.059	-0.108	-0.075	-0.106
$\alpha - 1$ (T4, [65])	0.048	-0.071	-0.065	-0.107	0.251	0.712
$\alpha - 1$ (T4, [66])	0.048	0.023	-0.058	-0.107	-0.075	-0.106

amplitudes, i. e. a value α closer to unity. Even bearing in mind the relatively large uncertainties in the numerically obtained amplitudes, this improvement is significant, at least for the (4, 3) and (5, 5) mode.

5. Conclusions

We have studied numerical simulations of a non-spinning black-hole binary system with mass-ratio $q = 4$ lasting about 11 orbits prior to coalescence. The numerical uncertainties for phase and amplitude due to discretization are $\Delta\phi \approx 0.6$ rad and $\Delta A/A \approx 1$ % for the quadrupole mode through inspiral, merger and ringdown when aligning the waveforms at the peak of the amplitude of the (2,2) multipole. The phase error is approximately constant, however, and we estimate the uncertainty for the purpose of a PN comparison closer to $\Delta\phi \approx 0.11$ rad. Numerical error due to wave extraction at finite radii results in larger uncertainties for the amplitude of about $\Delta A/A \lesssim 5$ % and a phase error $\Delta\phi \leq 0.2$ rad up to merger and 0.5 rad in the late ringdown stage. Uncertainties for subdominant multipoles are larger; approximately in proportion to the multipole index m for the phase and reaching 10 % to 25 % for higher-order modes in the amplitude. We also observe agreement within numerical uncertainties with an independent simulation of a $q = 4$ binary obtained with the BAM code.

We have performed a matching to post-Newtonian predictions using the Taylor T1 and T4 approximants and employing 3PN accurate expressions for the GW multipoles. Our main results in this comparison can be summarised as follows.

Using our numerical waveforms at finite extraction radii gives the misleading impression that Taylor T4 produces better agreement than the T1 approximant. Including subdominant multipoles with $l \neq m$ explicitly demonstrates the internal inconsistency of the numerical results at finite (too small) extraction radii: contrary to expectations the (2, 2) and (3, 2) as well as the (3, 3) and (4, 3) multipoles are significantly out of phase. This feature improves when going to larger radii and disappears when results are extrapolated to infinite radius. Subdominant modes thus provide valuable tests for the internal consistency of numerical results, irrespective of whether they are included in a comparison with post-Newtonian predictions or not.

By using extrapolated numerical results, we find the Taylor T1 approximant to provide better agreement with numerical results: using a matching window in the early inspiral, the accumulated phase error at $M\omega_{22} = 0.1$ is $\Delta\phi \approx 0.35$ rad for T1 compared with 1.0 rad for T4. For subdominant multipoles we obtain deviations of PN from NR results which to good approximation are proportional to the multipole index m .

The inclusion of higher-order PN terms in expressions for sub-dominant

multipoles in [66] leads to improved amplitude agreement with numerical results in our matching window covering approximately the frequency range $0.05 \leq M\omega \leq 0.06$. Even bearing in mind the relatively large numerical errors for the low amplitude modes, this improvement is significant at least for the (4, 3) and the (5, 5) multipole.

Acknowledgments

We thank Emanuele Berti for valuable discussions. C.F.S. and U.S. acknowledge support from the Ramón y Cajal Programme of the Spanish Ministry of Education and Science (MEC). U.S. acknowledges support by FCT-Portugal through Project No. PTDC/FIS/098025/2008, by grants from the Sherman Fairchild Foundation to Caltech and by NSF grants PHY-0601459, PHY-0652995, PHY-0960291. D.M. acknowledges support by the DFG Research Training Group 1523 “Quantum and Gravitational Field”. C.F.S. acknowledges support from a Marie Curie International Reintegration Grant No. MIRG-CT-2007-205005/PHY within the 7th European Community Framework Programme (EU-FP7) and contracts ESP2007-61712 (Spanish Ministry of Education and Science) and No. FIS2008-06078-C03-01/FIS (Spanish Ministry of Science and Innovation). This work was supported by allocations through the TeraGrid Advanced Support Program under Grant Nos. PHY-090003 and AST-100021 on the NICS Kraken and SDSC Trestles clusters, by an allocation through the Centro de Supercomputación de Galicia (CESGA) under project numbers ICTS-2009-120 and ICTS-CESGA-175 and Grant DECI-6 DyBHo by the EU-FP7 DEISA. This work was supported in part by DFG grant SFB/Transregio 7 “Gravitational Wave Astronomy” and the DLR (Deutsches Zentrum für Luft und Raumfahrt). BAM simulations were performed at HLRB2 of LRZ Munich.

References

- [1] J. Abadie *et al.* *Nucl. Instrum. Meth.*, A624:223–240, 2010.
- [2] VIRGO: <http://www.cascina.virgo.infn.it/advirgo/>.
- [3] M. Armano *et al.* *Class. Quant. Grav.*, 26:094001, 2009.
- [4] F. Pretorius. *Phys. Rev. Lett.*, 95:121101, 2005.
- [5] M. Campanelli, C. O. Lousto, P. Marronetti, and Y. Zlochower. *Phys. Rev. Lett.*, 96:111101, 2006.
- [6] J. G. Baker, J. Centrella, D.-I. Choi, M. Koppitz, and J. van Meter. *Phys. Rev. Lett.*, 96:111102, 2006.
- [7] Frans Pretorius. Binary Black Hole Coalescence. In M. Colpi *et al.*, editor, *Physics of Relativistic Objects in Compact Binaries: From Birth to Coalescence*. Springer, New York, 2009. arXiv:0710.1338 [gr-qc].
- [8] J. M. Centrella, J. G. Baker, B. J. Kelly, and J. R. van Meter. *Rev. Mod. Phys.*, 82:3069, 2010.
- [9] L. S. Finn. *Phys. Rev. D*, 46:5236, 1992.
- [10] P. Ajith *et al.* *Class. Quantum Grav.*, 24:S689–S700, 2007.
- [11] P. Ajith *et al.* *Phys. Rev. D*, 77:104017, 2008.
- [12] P. Ajith. *Class. Quant. Grav.*, 25:114033, 2008.
- [13] P. Ajith *et al.* 2009. arXiv:0909.2867 [gr-qc].
- [14] L. Santamaria *et al.* *Phys. Rev. D*, 82:064016, 2010.
- [15] R. Sturani *et al.* *J. Phys. Conf. Ser.*, 243:012007, 2010. arXiv:1005.0551 [gr-qc].
- [16] R. Sturani, S. Fischetti, L. Cadonati, G.M. Guidi, J. Healy, *et al.* 2010. arXiv:1012.5172 [gr-qc].
- [17] A. Buonanno and T. Damour. *Phys. Rev. D*, 59:084006, 1999.
- [18] T. Damour, A. Nagar, E. N. Dorband, D. Pollney, and L. Rezzolla. *Phys. Rev. D*, 77:084017, 2008.
- [19] T. Damour and A. Nagar. *Phys. Rev. D*, 77:024043, 2008.
- [20] T. Damour, A. Nagar, M. D. Hannam, S. Husa, and B. Brügmann. *Phys. Rev. D*, 78:044039, 2008.

- [21] M. Boyle *et al.* *Phys. Rev. D*, 78:104020, 2008.
- [22] T. Damour, M. Trias, and A. Nagar. *Phys. Rev. D*, 83:024006, 2011.
- [23] Y. Pan *et al.* *Phys. Rev. D*, 81:084041, 2010.
- [24] M. Hannam, S. Husa, F. Ohme, and Ajith P. *Phys. Rev. D*, 82:124008, 2010.
- [25] I. MacDonald, S. Nissanke, and H. P. Pfeiffer. 2011. arXiv:1102.5128 [gr-qc].
- [26] L. Lindblom, B. J. Owen, and D. A. Brown. *Phys. Rev. D*, 78:124020, 2008.
- [27] B. Aylott *et al.* *Class. Quantum Grav.*, 26:165008, 2009.
- [28] B. Aylott *et al.* *Class. Quantum Grav.*, 26:114008, 2009.
- [29] U. Sperhake. *Phys. Rev. D*, 76:104015, 2007.
- [30] A. Buonanno *et al.* *Phys. Rev. D*, 76:104049, 2007.
- [31] A. Buonanno, Y. Pan, H. P. Pfeiffer, M. A. Scheel, L. T. Buchman, and L. E. Kidder. *Phys. Rev. D*, 79:124028, 2009.
- [32] A. Buonanno, G. B. Cook, and F. Pretorius. *Phys. Rev. D*, 75:124018, 2007. gr-qc/0610122.
- [33] E. Berti *et al.* *Phys. Rev. D*, 76:064034, 2007.
- [34] E. Berti, V. Cardoso, J. A. González, U. Sperhake, and B. Brügmann. *Class. Quantum Grav.*, 25:114035, 2008. arXiv:0711.1097 [gr-qc].
- [35] M. Campanelli, C. O. Lousto, H. Nakano, and Y. Zlochower. *Phys. Rev. D*, 79:084010, 2008.
- [36] S. Brandt and B. Brügmann. *Phys. Rev. Lett.*, 78:3606–3609, 1997.
- [37] J. M. Bowen and J. W. York, Jr. *Phys. Rev. D*, 21:2047–2056, 1980.
- [38] M. Ansorg, B. Brügmann, and W. Tichy. *Phys. Rev. D*, 70:064011, 2004.
- [39] H. P. Pfeiffer, D. A. Brown, L. E. Kidder, L. Lindblom, G. Lovelace, and M. Scheel. *Class. Quantum Grav.*, 24:S59–S82, 2007.
- [40] J. Thornburg. *Phys. Rev. D*, 54:4899–4918, 1996.
- [41] J. Thornburg. *Class. Quantum Grav.*, 21:743–766, 2004.
- [42] J. A. González, U. Sperhake, B. Brügmann, M. D. Hannam, and S. Husa. *Phys. Rev. Lett.*, 98:091101, 2007.
- [43] U. Sperhake, E. Berti, V. Cardoso, F. Pretorius, and N. Yunes. *Phys. Rev. D*, 83:024037, 2011.
- [44] U. Sperhake, E. Berti, V. Cardoso, J. A. González, B. Brügmann, and M. Ansorg. *Phys. Rev. D*, 78:064069, 2008.
- [45] Cactus Computational Toolkit homepage: <http://www.cactuscode.org/>.
- [46] E. Schnetter. *Class. Quantum Grav.*, 20:4719, 2003.
- [47] Carpet Code homepage: <http://www.carpetcode.org/>.
- [48] M. Shibata and T. Nakamura. *Phys. Rev. D*, 52:5428–5444, 1995.
- [49] T. W. Baumgarte and S. L. Shapiro. *Phys. Rev. D*, 59:024007, 1998.
- [50] J. R. van Meter, J. G. Baker, M. Koppitz, and D.-I. Choi. *Phys. Rev.*, D73:124011, 2006.
- [51] D. Müller and B. Brügmann. *Class. Quantum Grav.*, 27:114008, 2010.
- [52] E. Schnetter. *Class. Quantum Grav.*, 27:167001, 2010.
- [53] D. Müller, J. Grigsby, and B. Brügmann. *Phys. Rev. D*, 82:064004, 2010.
- [54] D. Alic, L. Rezzolla, I. Hinder, and P. Mösta. *Class. Quantum Grav.*, 27:245023, 2010.
- [55] B. Brügmann, J. A. González, M. D. Hannam, S. Husa, U. Sperhake, and W. Tichy. *Phys. Rev. D*, 77:024027, 2008.
- [56] D. Brown *et al.* 2007. arXiv:0709.0093 [gr-qc].
- [57] C. Reisswig and D. Pollney. 2010. arXiv:1006.1632 [gr-qc].
- [58] B. Vaishnav, I. Hinder, F. Herrmann, and D. Shoemaker. *Phys. Rev. D*, 76:084020, 2007. arXiv:0705.3829.
- [59] M. Boyle *et al.* *Phys. Rev. D*, 76:124038, 2007.
- [60] M. D. Hannam, S. Husa, J. A. González, U. Sperhake, and B. Brügmann. *Phys. Rev. D*, 77:044020, 2008.
- [61] B. Brügmann, W. Tichy, and N. Jansen. *Phys. Rev. Lett.*, 92:211101, 2004. gr-qc/0312112.
- [62] M. Hannam, S. Husa, F. Ohme, D. Müller, and B. Brügmann. *Phys. Rev. D*, 82:124008, 2010.
- [63] A. H. Mroue, H. P. Pfeiffer, L. E. Kidder, and S. A. Teukolsky. *Phys. Rev. D*, 82:124016, 2010.
- [64] L. Blanchet. *Living Reviews in Relativity*, 9(4), 2006. <http://www.livingreviews.org/lrr-2006-4>.
- [65] L. E. Kidder. *Phys. Rev. D*, 77:044016, 2008.
- [66] L. Blanchet, G. Faye, B. R. Iyer, and S. Sinha. *Class. Quant. Grav.*, 25:165003, 2008.
- [67] J. A. Nelder and R. Mead. *Computer Journal*, 7:308–313, 1965.
- [68] Press, William H. and Teukolsky, Saul A. and Vetterling, William T. and Flannery, Brian P. *Numerical recipes in C (2nd ed.): the art of scientific computing*. Cambridge University Press, New York, NY, USA, 1992.
- [69] C. Reisswig, N. T. Bishop, D. Pollney, and B. Szilagyi. *Phys. Rev. Lett.*, 103:221101, 2009.
- [70] C. Reisswig, N. T. Bishop, D. Pollney, and B. Szilagyi. *Class. Quantum Grav.*, 27:075014, 2009.
- [71] M. C. Babiuc, B. Szilagyi, J. Winicour, and Y. Zlochower. 2010. arXiv:1011.4223 [gr-qc].

[72] M. Boyle and A. H. Mroué. *Phys. Rev. D*, 80:124045, 2009.